Prediction of particulate characteristics in an expanding laser plume

Dustin Blair[a] , Mark Tillack[a] and Mofreh Zaghloul[a]

[a]University of California at San Diego, Energy Technology Group *

ABSTRACT

We present a mathematical model of particulate formation and dynamics in the laser ablation plume. This model is presented in a practical layout and applied to an example problem predicting the behavior of silicon, a material commonly used in the fabrication of microdevices. Additionally, we examine an intermediate intensity regime of laser ablation, in which there are multiple cooling mechanisms that can be considered important, but plume ionization is not significant. Results are discussed with an emphasis on pulsed laser ablation manufacturing processes, which often take place at atmospheric pressure. Important observations derived from this work are as follows: 1) The plume is quickly condensed and stopped in less than a microsecond in a distance of less than a millimeter at atmospheric pressure. 2) Particulates predicted by this model are on the order of $10\mathring{A}$ in diameter, the majority of which condense back onto the target surface.

Keywords: C ondensation, Plume, Laser, Ablation

1. INTRODUCTION

The particles condensed out of laser ablation plume vapor along with those released via hydrodynamic sputtering create problems in the production of microdevices utilizing laser machining techniques. These particles can unpredictably attenuate incident laser energy in subsequent pulses. Temporal (shot to shot) and spatial energy intensity variations caused by the remnant particles of a previous plume are currently believed to be a source of significant process variability. Additionally, vapor condensation on the workpiece itself creates quality problems, which necessitate the use of secondary cleaning processes to achieve satisfactory quality levels.

Lasers can also be used in the production of nanoscale particles. Present techniques for nanoscale particle synthesis are based on the phenomenon of homogenous nucleation in the gas phase by methods such as plasma arc, high-frequency discharge, magnetron sputtering, vaporization of materials in vacuum chamber, chemical vapor deposition, and electron beam methods. Considerable efforts are made to obtain monodispersed particles since narrow size distribution is regarded as a necessary condition for high quality nanoparticle manufacturing. Laser techniques for particle synthesis have several advantages. They allow an easy control of the evaporation process and do not require an enclosure for the evaporated substance.

The vapor ejected by laser radiation usually supercools because of its expansion and interaction with the cold ambient gas. The supercooled vapor condenses partially on the target surface and partially in the gas phase, in the form of nanoscale particles. At high laser flux density or low ambient gas pressure, a supersonic vapor flow is formed where adiabatic expansion is the predominant cooling mechanism. At lower laser flux densities, a subsonic vapor jet is created where heat conduction and diffusion mixing with an ambient gas are the predominant cooling mechanisms. Condensation conditions such as cooling rate and vapor density strongly differ at different points in the jet and, as a consequence, the size of the synthesized particles can vary over more than one order of magnitude, maximum to minimum size ratio. Previous authors generally focus on one regime or the other. In the present work, we consider the regime in which laser machining processes generally take place and offer an intuitive physical explanation, which should help the process engineer in understanding the physics underlying laser processing techniques.

The work described herein helps to lay the foundation of basic research supporting the optimization of pulsed laser ablation processing in microfabrication as well as the production of high quality nanoparticles.

*Contact information: Send correspondence to UC San Diego, 460 EBU-II, mail code 0417, La Jolla, CA 92093-0417, email: dustin_ blair@hp.com, Telephone: 858.655.8162

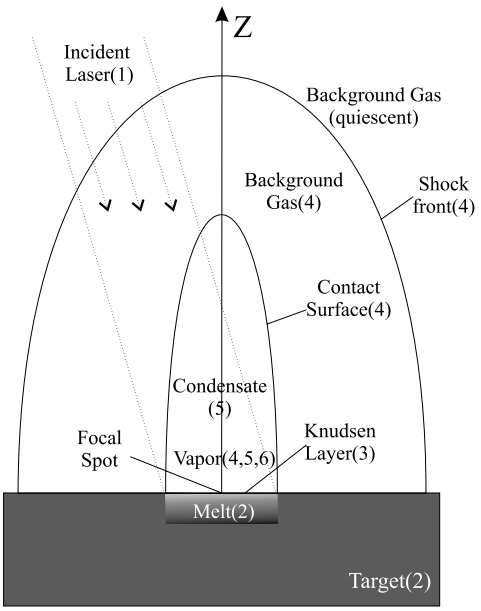

Figure 1. Configuration of the Laser Ablation Experiment. Numbers indicate corresponding section(s) within this paper.

This paper is broken into several sections for clarity. 2) Temperature Distribution in the Target; 3) Conditions at the Flow-Target Boundary; 4) Expansion Dynamics; 5) Particulate formation; 6) Transport Properties; 7) Method of solution; 8) Results; and 9) Conclusions.

For illustrative purposes, an example problem is solved using the proposed model. The example consists of a silicon target in argon background gas at atmospheric pressure, which is ablated with a laser. Incident laser energy is in the form of a 532nm, Gaussian(in time), 10nsec (full width half maximum) pulse peaking at $7 \times 10^{12} W/m^2$.

2. TEMPERATURE DISTRIBUTION IN THE TARGET

The purpose of this section is to describe the flow of energy within the ablation target. For the sake of modeling simplicity, several idealizations of the laser induced boundary influx flow are assumed: 1) the laser intensity is a simple Gaussian profile in time and uniform in space; 2) vaporization is driven by an energy balance between incident energy, conduction and target energy flux due to vaporization; 3) incident energy absorption is calculated using a surface reflectivity coefficient varied as a function of target temperature, which is estimated from experimental data; 4) the surface recession rate is very slow compared to the gas efflux velocity.

The steady-state recession rate of the target is $\rho_g u_g / \rho_l$, where the subscripts g and l refer to gas and liquid. Therefore, the last assumption is valid if $\rho_g \ll \rho_l$, as is typically true.

For the problem currently under study, target heating can be satisfactorily modeled using a 1-D approximation due to the fact that the thermal diffusion distance is much smaller than the lateral dimension of the laser beam in the regime of interest here. For the example problem in silicon, thermal diffusion characteristic lengths $d = \sqrt{\kappa t}$ are on the order of 1um for a 10nsec laser pulse (κ is target thermal diffusivity). This assumption should continue to be valid as characteristic dimensions shrink as long as shorter pulses are employed, as is the current trend.

Starting with the 1-D heat conduction equation:

$$\lambda_t \partial^2 T(z,t)/\partial z^2 + A(z,t) = \rho C_p \partial T(z,t)/\partial t \tag{1}$$

with

$$A(z,t) \cong I_{abs}(t)\alpha e^{-\alpha z} \tag{2}$$

where $A(z,t)$ represents the absorbed laser energy density with α being the extinction coefficient for the target material at the laser wavelength. I_{abs} is the absorbed energy flux and λ_t is the target thermal conductivity, which is estimated as a function of temperature using values derived from experiment. α is the spatial absorption coefficient for the target material at the laser wavelength.

I_{abs} can be found using the simple expression $I_{abs} = (1-R)I_o$, where I_o is the incident irradiance. R is the surface reflectivity, estimated using the functional relationship $1 - R = (1-R)_o + aT$. a is a constant estimated from experimental data.[1]

Energy flux out of the target surface due to vaporization at $z = 0$ is represented by the following relationship.[2]

$$B = u(\rho_v Q_v + E + \rho_v u^2/2 + p) \tag{3}$$

Where Q_v is the target heat of evaporation and ρ_v is the vapor density. E is the internal energy of the ejected vapor and p, it's pressure.

The thermal response within the target is estimated using finite difference approximation of equation 1. Target cooling after laser pulse termination is estimated similarly, assuming no incident laser energy.

3. CONDITIONS AT THE FLOW-TARGET BOUNDARY

Having determined the temperature distribution in the target as described in the previous section, conditions at the target-flow boundary can now be estimated.

Following Kelly et al,[1] the vapor pressure can be estimated via classical thermodynamic expressions, which can be used to derive an expression relating temperature to vapor pressure known as Clausius-Clapeyron's Law(4).

$$P_s = P_o exp[Q_v/(kT_b) - Q_v/(kT_s)] \tag{4}$$

T_b is the boiling temperature of the target material at P_o ambient pressure with k being the Boltzmann constant. T_s is the target surface temperature at melt-vapor interface.

Another condition set at the target boundary is the absence of background gas flux into the flow space with N_g, the background gas density:

$$N_g u = 0, z = 0 \tag{5}$$

At the target surface, the gas near the phase interface is not in translational equilibrium when the evaporation rate is large, as is the case in the laser intensity regime of interest here. To realistically represent the conditions at the target-flow boundary, a Knudsen layer model is employed, which treats that region as a gasdynamic discontinuity across which certain jump conditions expressing conservation of mass, momentum and energy are applied.

Translational equilibrium is achieved within a few mean free paths by collisions between particles in a Knudsen layer region. Changes in flow properties can be described as jump conditions across the Knudsen layer, simplified for a monatomic gas($\gamma = 5/3$)[3]:

$$\left(\frac{T_k}{T_s}\right)^{1/2} = \left(1 + \frac{\pi s^2}{64}\right)^{1/2} - \frac{(\pi)^{1/2}}{8}s \tag{6}$$

$$\frac{P_k}{P_s} = \left(\frac{T_k}{T_s}\right)^{1/2}\left[\left(s^2 + 1/2\right) erfc(s) \cdot exp(s^2)\right. \tag{7}$$
$$\left. - \frac{s}{(\pi)^{1/2}}\right] + \frac{1}{2}[1 - (\pi)^{1/2} s \cdot erfc(s) \cdot exp(s^2)]$$

Which represent the conservation of mass, momentum and energy across the Knudsen layer, taking into account particle backscattering.

Where $\rho_k = \rho_v(0,t)$, $T_k = T(0,t)$, $P_k = P(0,t)$, and $u_k = u(0,t)$ are vapor parameters at the outer edge of the Knudsen layer, $T_s = T_t(0,t)$ is the surface temperature, P_s is the saturated vapor pressure given by equation 4 and $s = u_k/(2kT/m_v)^{1/2}$ is the dimensionless speed ratio. ρ_s is properly interpreted as the saturated vapor density at the liquid temperature T_s. m_v is the atomic mass of the ejected vapor.

During the laser pulse, if the intensity is sufficiently high, nonequilibrium processes within the Knudsen layer drive the flow to sonic velocity in that zone. If the saturated vapor pressure is high enough, there is a centered rarefaction fan in the flowfield which takes the sonic flow outside the Knudsen layer to supersonic speed. The sonic nature of the flow just beyond the Knudsen layer becomes the velocity boundary condition during the period where the saturated vapor pressure is sufficiently intense. According to Knight,[3] the criteria for sonic escape velocity beyond the Knudsen layer can be stated as (8), where Q_v is the heat of vaporization on a per unit mass basis and q represents the heat flows from the incident laser and losses to conduction within the target.

$$\frac{q_i - q_c}{Q_v \rho_s \sqrt{RT_s/2\pi}} = 0.816 \tag{8}$$

Which results from the following energy balance, allowing an estimation of the flow velocity beyond the expansion fan.

$$q_i = q_c + \rho_s u Q_v \tag{9}$$

Using the preceding reasoning and considering the laser intensity regime of interest here, the flow is found to be sonic exiting the Knudsen layer region during the laser pulse. At the end of the laser pulse, the target begins to cool rapidly, allowing a simplified boundary condition at the target surface contiguous with the vapor.[4]

$$u = -\left(\frac{5kT}{3m_v}\right)^{1/2} \tag{10}$$

The above equation requires vapor movement toward the surface with a velocity of the local sound speed, which also implies the assumption of complete vapor condensation at the cooling target surface.

4. EXPANSION DYNAMICS

This section describes the evolution of the vapor plume into the background gas. A simplification of the vapor-condensate flow problem is assumed, where the gas-liquid flow is essentially homogeneous. The main consequence of this simplification is that the condensate momentum can only be estimated via the momentum of the overall mixture. The main idealizations adopted under this model are:

1) The vapor and condensed phases are at the same velocity and temperature, therefore do not exchange momentum with one another. 2) The two-phase flow behaves like a single phase having fluid properties whose values are, in some sense, mean values for the flow. 3) Condensed mass does not impact the overall dynamics of the flow, hence does not appear in the mixture momentum equation. 4) Condensed particulates do not alter the transport properties in the plume. 5) Emission and absorbtion of radiant energy are neglected.

It is also estimated that the vapor is cold enough to be essentially transparent[5] and the vapor diffusion length is much smaller than the beam diameter. The considered processes are characterized by high temperature and concentration gradients. Therefore, the phenomena of heat conduction and diffusion of vapor into surrounding ambient gas are taken into account.[6]

The equations of continuity, vapor transport, momentum and energy for a binary mixture are as follows[7]:

$$\frac{\partial \rho}{\partial t} + \nabla \cdot (\rho \overline{v}) = 0 \tag{11}$$

$$\frac{\partial (\rho_v)}{\partial t} + \nabla \cdot (\rho_v \overline{v}) = \nabla \cdot \rho D_{ab} \nabla \omega - m_v I_n \tag{12}$$

$$\frac{\partial \rho \overline{v}}{\partial t} = -\nabla \cdot [\rho \overline{v}\overline{v} + \widetilde{\pi}] \tag{13}$$

$$\frac{\partial \rho (\widehat{U} + \frac{1}{2} v^2)}{\partial t} = -(\nabla \cdot e) - Q_v I_n \tag{14}$$

where

$$e = \rho [\widehat{U} + \frac{1}{2} v^2] \overline{v} + q + [\widetilde{\pi} \cdot \overline{v}] \tag{15}$$

and $\widetilde{\pi}$ represents the pressure tensor, which is the sum of the pressure and the viscous part of the momentum flux(or shear stress tensor). $\omega = \rho_v / \rho$ is the mass density fraction, $\widehat{U}$ is the internal energy per unit mass and D_{ab} is the binary diffusivity for the vapor-ambient system. Here, q represents the conductive and diffusive energy flux relative to the mass average velocity of the mixture.

I_n is the vapor condensation rate, which is described in the following section on particulate formation and found in equation 18. It is through this quantity that the flow physics are coupled to condensation physics due to the fact that it describes the transition of mass from vapor to condensate. I_n also appears in the energy equation in order to account for the heat of condensation released upon the formation and growth of clusters.

The above equations describe the flow of mass, momentum and energy throughout the flow space as represented in Figure 1. The boundary conditions are atmospheric pressure and standard room temperature at the end of the modeled space opposite the target. Initially, the surrounding ambient gas is assumed uniform and quiescent.

5. PARTICULATE FORMATION

This section puts forth the modeling which describes condensate cluster nucleation and growth. The modeling is based on Zeldovich-Raizer theory, which has been applied to describe a wide range of condensation problems.[8] The following assumes an absence of foreign nucleants to which vapor molecules can adhere. In this situation, phase transition from vapor to liquid is blocked by a free-energy barrier, which comes from the appearance of new surface when embryos of the new phase start to form.

In the presence of ions, the speed of production of nuclei must be modified to account for the different potential associated with cluster formation, so the ionization state of the ejected vapor must be considered. Assuming local thermodynamic equilibrium, we can use the Saha equation to estimate the degree of ionization of the vapor.[9] For the example problem with laser intensity below $10^{13} W/m^2$, it was determined that the ionization fraction is small throughout the flow space, which indicates it safe to assume neutral flow without causing significant errors in the prediction of the condensation rate.

After passing through the saturation stage, the vapor continues to cool, following the Poisson adiabat, and becomes supersaturated. The speed of formation of the nuclei of the liquid phase depends very strongly on the

degree of supersaturation, and therefore the number of produced condensation centers increases very rapidly with increasing supersaturation. At the maximum supersaturation, the speed of condensation becomes such that the liberation of latent heat stops the increase in supersaturation. Moreover, the condensation accelerates even if the number of condensation centers is constant, owing to the increase in surface area to which vapor molecules can adhere. Therefore, the accelerating condensation not only slows the rise in supersaturation, but ultimately reverses it. The formation of new nuclei, which is exceedingly sensitive to the magnitude of supersaturation, immediately ceases and condensation from now on proceeds via adhesion of vapor molecules to drops already present. Thus, all the condensation centers are generated at the beginning of the process, directly after the saturated state is reached. Their number depends on the maximum degree of supersaturation attained, which in turn is determined by the interplay between two opposite influences: cooling of the vapor due to the work of expansion, and heating of the vapor due to the latent heat liberated during condensation.

As the spacings between vapor atoms become large relative to the mean free path in the vapor, acts of adhesion become too rare; the rate of adhesion, which is proportional to the density, i.e. $\sim t^{-3}$, is no longer capable of "following" the expansion leading to so called quenching. Soon the condensation ceases completely and the residue of the gas (together with the drops) is again cooled rapidly along the Poisson adiabat.

Under stationary conditions and in the absence of ions, the speed of production of nuclei is known to be[10]

$$G = \frac{2N_v^2}{N_c}\Big(\frac{\sigma}{2\pi m_v}\Big)^{1/2} e^{-\frac{b}{\theta^2}} \tag{16}$$

where σ is the surface tension, N_c is the number density in the condensed phase, N_v is the number density in the vapor phase and the coefficient b is

$$b = \frac{16\pi}{3}\frac{\sigma^3}{N_c^2 Q_v^2 kT} \tag{17}$$

The condensation rate I_n (number of vapor molecules which are condensed inside a unit volume per unit time) is the sum of the vapor molecules consumed per nucleation and the condensation flux onto the collective surface area of all existing particulates.

$$I_n = 4\pi J \int_0^\infty F(R)R^2 dR + \frac{4}{3}\pi r_*^3 N_c G \tag{18}$$

The condensation flux is given by the Knudsen formula[11]

$$J = \frac{Px - P_s}{\sqrt{2\pi m_v kT}} \tag{19}$$

where the saturated vapor pressure P_s is given by equation 4, which is derived from the Clausius-Clapeyron equation under the assumption that Q_v does not depend on T (T_b is the boiling temperature at $P_o = 1atm$).[8]

θ is the degree of supercooling or supersaturation, which is connected with the radius r^* of a critical nucleus containing $g^* = 4\pi r^{*3}/3v_b$ molecules by the condition for maximum thermodynamic potential:

$$\theta = (T_{eq} - T)/T_{eq} = 2\sigma/(N_c Q_v r^*) \tag{20}$$

where T_{eq} is the temperature of vapor saturated at a given vapor density. v_b is the volume per particle in the condensed phase and P_v is the pressure in the condensing vapor.

$$T_{eq} = \Big[\frac{1}{T_b} - \frac{k}{Q_v} ln\Big(\frac{P_v}{P_o}\Big)\Big]^{-1} \tag{21}$$

The rate of growth of a supercritical drop equals the difference between the rates of adhesion and evaporation of the molecules. This calculation neglects, as an approximation, the difference between the evaporation from a drop and the evaporation from a flat liquid surface(this does not exaggerate the rate of growth of the droplet greatly[8]). In addition, this calculation also assumes the temperature of the droplet coincides with the that of the vapor(the heat of condensation is dissipated rapidly by a small droplet).

Following Gnedovets et al,[11] the size distribution of condensate particles $F(R, Z, t)$ (FdR is the number of particles with radius from R to $R + dR$ in a unit volume) is determined by the transport equation

$$\frac{\partial F}{\partial t} + \nabla \cdot FU + \frac{\partial FL}{\partial R} = 0 \tag{22}$$

where $L = J/N_c$ is the linear growth rate of a particle.

6. TRANSPORT PROPERTIES

The values of thermal conductivity, λ_o and viscosity, μ_o were derived from experimental data for argon and for the silicon target. Values for silicon vapor were estimated using kinetic theory.[12] Variations of transport coefficients with temperature are estimated for the mixture using the following relationships.

$$\lambda = \lambda_o \Big(\frac{T}{T_o}\Big)^{1/2} \tag{23}$$

which can be estimated for the multi-component mixture using

$$\lambda_{mix} = \Sigma \omega_i \lambda_i \tag{24}$$

Viscosity of the mixture is treated similarly in order to estimate mixture variation with temperature.

$$\mu = \mu_o \Big(\frac{T}{T_o}\Big)^{1/2} \tag{25}$$

The interdiffusion coefficient was estimated from molecular masses and molecular diameters by means of Chapman-Enskog theory. To a first-order approximation for molecules (rigid spheres) the diffusion coefficient is given by

$$D_{ab} = \frac{2}{3}\Big(\frac{k^3}{\pi^3}\Big)^{1/2}\Big(\frac{1}{2M_a} + \frac{1}{2M_b}\Big)^{1/2}\frac{T^{3/2}}{P(\frac{d_a+d_b}{2})^2} \tag{26}$$

where M is the molecular mass and d is the molecular diameter of the vapor and background gas.

7. METHOD OF SOLUTION

In order to obtain the spatial distribution of the condensed phase numerically, it is useful to break the condensate distribution function down into a system of moments, for which a series of transport equations can be solved.

Following Gnedovets et al,[11] the transport equation (22) is transformed to an infinite set of moment equations by multiplying by R^k and integrating over R from zero to infinity.

For $k = 0$

$$\frac{\partial F_k}{\partial t} + \frac{\partial F_k U}{\partial z} = G \tag{27}$$

where G is the nucleation rate (number of nuclei formed in a unit volume per unit time) derived using equation 16.

For $k = 1, 2, 3, \ldots$

$$\frac{\partial F_k}{\partial t} + \frac{\partial F_k U}{\partial z} = kLF_{k-1} \tag{28}$$

where the moments are defined as

$$\int_0^\infty FR^k dR \tag{29}$$

An integral particle-size distribution (that can be experimentally observed) is given by

$$H(R) = \int_0^\infty F(R, z) dz \tag{30}$$

where HdR is the number of particles with a radius from R to R + dR formed per unit area of irradiated surface. A local particle-size distribution F at any z can be approximated by the Gaussian function because the standard deviation is much less than the mean particle size.

The hydrodynamic equations are reduced to one spatial dimension in order to make the problem more tractable. The $1D$ equations of continuity, vapor transport, momentum and energy for a binary mixture are as follows[7]:

$$\frac{\partial \rho}{\partial t} + \frac{\partial (\rho u)}{\partial x} = 0 \tag{31}$$

$$\frac{\partial (\rho_v)}{\partial t} + \frac{\partial (\rho_v u)}{\partial z} = \frac{\partial}{\partial z}(\rho D_{ab} \frac{\partial \omega}{\partial z}) - m_v I_n \tag{32}$$

$$\frac{\partial \rho u}{\partial t} = -\frac{\partial \rho u u}{\partial z} - \frac{\partial}{\partial z} \mu \frac{\partial u}{\partial z} - \frac{\partial p}{\partial z} \tag{33}$$

$$\frac{\partial e}{\partial t} = -\frac{\partial e u}{\partial z} - \frac{\partial q}{\partial z} + \mu \left(\frac{\partial u}{\partial z}\right)^2 + \frac{\partial p}{\partial t} + u \frac{\partial p}{\partial z} + Q_v I_n \tag{34}$$

where

$$e = \rho \widehat{C_p} T \tag{35}$$

and

$$q = -\lambda \frac{\partial T}{\partial z} - \sum H \rho D_{ab} \frac{\partial \omega_i}{\partial z} \tag{36}$$

where μ represents the viscosity of the mixture, derived using means previously discussed. ω is the mass density fraction $\omega = \rho_v / \rho$, e is the internal energy per unit volume and D_{ab} is the binary diffusivity for the vapor-ambient system. H is the component enthalpy on a mass basis.

The above equations describe the flow of mass, momentum, energy and condensate distribution throughout the computational space as represented in Figure 1. Numerically, the system of equations was solved using an explicit Euler scheme forward stepping in time. Spatial derivatives were approximated with simple upwind differencing to avoid oscillations in the solution, which can result in singularities in the condensation model.

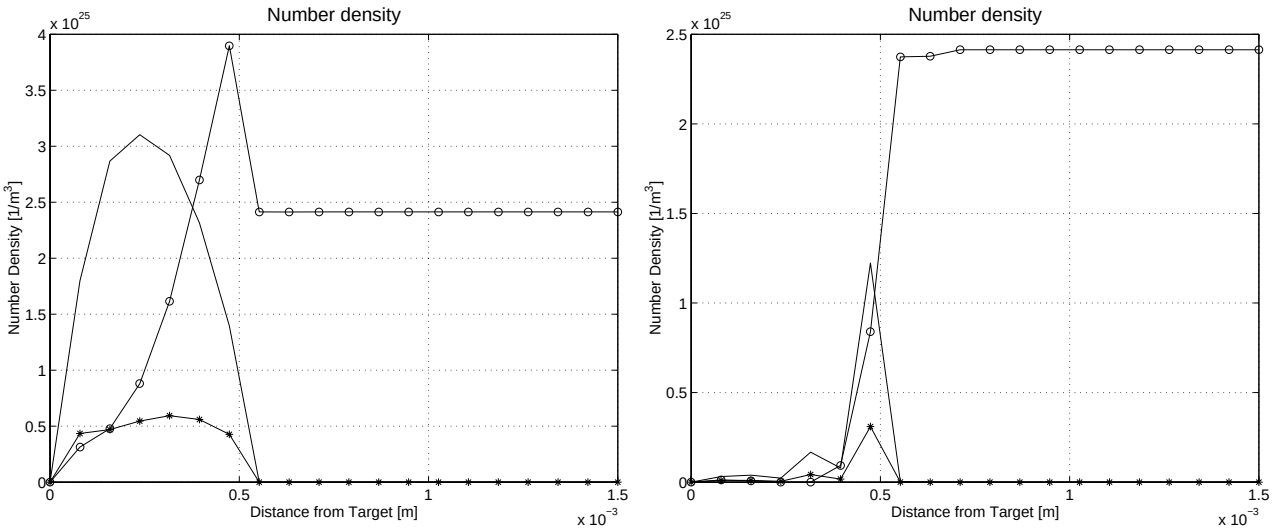

Figure 2. Spatial number density distributions of ejected vapor(-), condensate×10(*) and background gas(o) at t=100 and 800 nsec.

8. RESULTS

The results of the numerical simulation of the example problem (a silicon target in an argon ambient background gas at 1 atm) are presented in the following figures. Incident laser energy is in the form of a Gaussian 10nsec (full width half maximum) pulse peaking at $7 \times 10^{12} W/m^2$.

Figure 2 represents the spatial distributions of the different types of mass in the system, vapor, background gas, and condensate. These figures illustrate the transition from vapor to condensate in less than $1 \mu sec$, which quickly drives the vapor pressure, hence total pressure, down to miniscule levels. The vapor also rapidly pushes the background gas away from the target, creating a pressure wave which propagates outward from the target. The contact surface is blurred over time as diffusion takes place, allowing the vapor and background gases to merge with one another as the vapor condenses.

It is also apparent in figure 2 that condensate particles do not reside near the target surface as the simulation progresses, which is due to the fact that vapor near the target surface preferentially condenses back onto the target, keeping the target heated in the process via the vapor's heat of condensation. Through this recondensation process, the majority of the vapor initially ejected eventually finds itself back on the target, dragging with it the condensate clusters.

The dependence of the homogeneous nucleation rate on spatial coordinates has a sharp maximum (fig. 3), which can be considered a nucleation front inside which the nuclei are formed. Particles grow behind this front, which indicates that the nucleation and condensation processes are separated in space somewhat. This front can be seen to coincide with the contact surface between the vapor and the background gas, where diffusion serves to cool the vapor and accelerate the condensation process.

Variation in target surface temperature results from an imbalance between incident laser energy and losses due to conduction into the target and energy lost to the outflow of vaporized target material. Target temperature is driven substantially by the flow of incoming laser energy, which is readily apparent in figure 4.

Figure 5 shows the evolution of the flow mixture temperature distribution through time. The peak at the outer edge of the temperature distribution at 800 nsec results from the heat of condensation released by the last remaining growing condensate particles within the expanding plume. Early in the flow evolution, condensation and growth are confined to the leading edge of the contact surface, where diffusive and conductive cooling effects drive the temperature down sufficiently that significant condensation may occur.

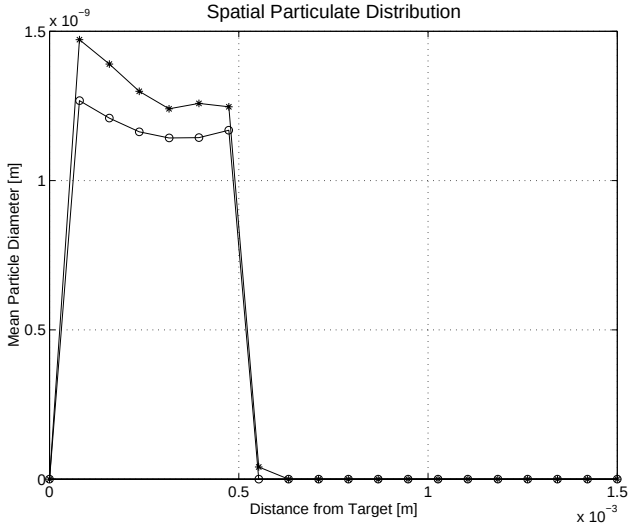

Figure 3. Spatial condensate radial distribution at 100(o) and 400nsec(*).

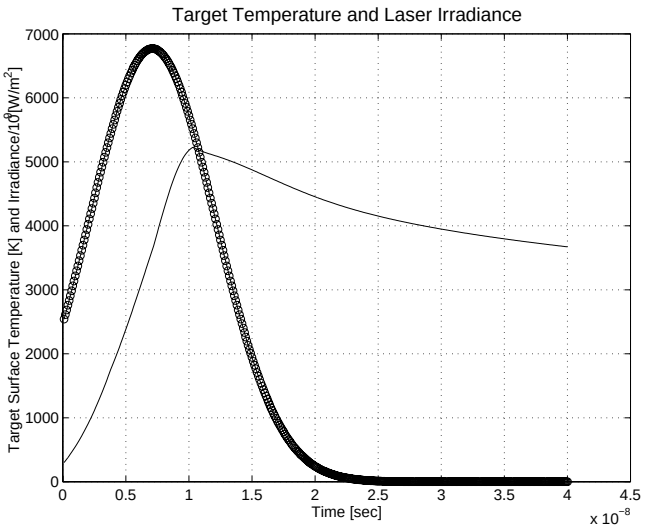

Figure 4. silicon target surface temperature(-) and Laser Irradiance(o) as a function of time.

Additionally, the Zeldovich-Raizer model predicts excessive nucleation at very high degrees of supersaturation which exist in a vapor plume rapidly expanding and cooling into a background gas.[13] At degrees of supersaturation greater than about 0.2, the theory predicts a critical radius smaller than a single atom. This is just another way of saying that any cluster formed in the vapor is stable, even those as small as two atoms. The problem is that the predicted nucleation rate at these conditions gives an excessively large number for the birthrate of legitimate clusters by about two orders of magnitude. It is also expected that the macroscopic condensation theory will not apply precisely to clusters made up of only 2 atoms. One simple correction is that the nucleation rate can be limited to the prediction of clusters no smaller than two atoms to give a more accurate result, which was the approach taken here.

Condensation results in a rapid decrease in the vapor pressure of the ablated material, which explains the short plume stopping distances typically observed in laser ablation at atmospheric pressure. That also explains

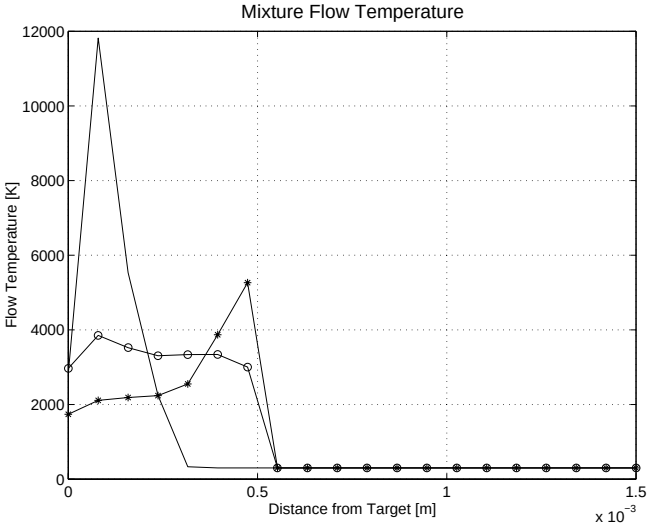

Figure 5. Flow temperature distribution at 20(-), 100(o) and 800(*) nsec.

the observation that so much of the ejected vapor ends up back on the target surface. The ultimate collapse of the vapor plume under ambient atmospheric pressure suggests that, under these conditions, the majority of the ablated material will ultimately be pulled back onto the target. This observation makes ablation in a high pressure background gas a potentially useful process for the intentional deposition of nanoparticles onto a substrate of like material. At the same time, production processes involving high pressure ambient gases do not appear optimum in terms of workpiece cleanliness. This would be better accomplished in a rarified atmosphere, where plume remnants are carried further by their initial momentum, hence might be carried off in a cleansing flow.

The current model does not take into account collisions between clusters, which would increase the size of the experimentally observed particulate distribution. An expected outcome of this effect would be a more bimodal distribution, with combined clusters forming the larger mode.[14]

9. CONCLUSIONS AND FUTURE WORK

A system of 1D equations was numerically solved to estimate the characteristics of particulates generated when machining with lasers in an inert background gas at atmospheric pressure. The interaction between the laser and the target was simplified in order to focus on the nucleation and flow physics as well as the resulting particle distribution.

Important observations derived from this work are as follows: 1) The plume is quickly condensed and stopped in less than a microsecond in a distance of less than a millimeter at atmospheric pressure. 2) Particulates predicted by this model are on the order of $10\mathring{A}$ in diameter, the majority of which condense back onto the target surface. 3) This model, which does not explicitly calculate condensate momentum, cannot predict the collapse of the background gas onto the target surface, hence the spatial distribution of particulates as $time \rightarrow \infty$. 4) The inclusion of diffusion, thermal conductivity and viscosity in this model does not substantially alter the predicted plume stopping distance, density and radial distribution for the purposes of engineering calculations.

The model breaks down at the later stages of plume evolution as $\rho_v \rightarrow 0$, since there is no vapor left in the flow. There exists no information regarding the momentum of the condensate, which is considered only in terms of creating a mass deficit in the vapor. This suggests a modification to the model in which a momentum equation is added for the condensate as well as a means of momentum exchange with the remaining gaseous mixture.

Improving the simulation of laser-target coupling and radiation transport at higher laser intensities will be the subject of future work as will be the experimental validation of present results. Additionally, the explicit

treatment of the exchange of momentum between condensed particulates and the gaseous background mixture will be examined in order to extend the applicability of the model to late stage plume collapse.

Acknowledgments

The work was supported by the University of California under a Department of Energy grant and Hewlett Packard Company.

REFERENCES

1. R. Kelly, "Laser-sputtering-part III. the mechanism of the sputtering of metals low energy densities," *Nucl. Instr. And Meth. B 7/8* , pp. 755–763, 1985.
2. A. Gusarov, A. Gnedovets, and I. Smurov, "Two-dimensional gas-dynamic model of laser ablation in an ambient gas," *Applied Surface Science* **154-155**, pp. 66–72, 2000.
3. C. Knight, "Theoretical modeling of rapid surface vaporization with back pressure," *AIAA J* **17**, pp. 519–523, 1979.
4. K. Chen, J. Leboeuf, R. Wood, D. Geohagen, J. Donato, C. Liu, and A. Puretzky, "Accelerated expansion of laser-ablated materials near a solid surface," *Physical Review Letters* **75**, pp. 4706–4709, 1995.
5. J. Leboeuf, K. Chen, J. Donato, D. Geohagen, C. Liu, A. Puretzky, and R. Wood, "Dynamical modeling of laser ablation processes," *http://exodus.physics.ucla.edu/leboeuf/mrs1995.pdf* , pp. 1–12, 1995.
6. H. Le, D. Zeitoun, J. Parisse, M. Sentis, and W. Marine, "Modeling of gas dynamics for a laser-generated plasma: Propagation into low-pressure gases," *Physical Review E* **62**, pp. 4152–4161, 2000.
7. R. Bird, W. Stewart, and E. Lightfoot, *Transport Phenomena*, John Wiley New York, 1960.
8. Y. Zeldovich and Y. Raizer, *Physics of Shock Waves and High-Temperature Hydrodynamic Phenomena*, Academic Press, 1967.
9. F. Chen, *Plasma Physics and Controlled Fusion*, Plenum Press, 1984.
10. J. Frenkel, *Kinetic Theory of Liquids*, Dover Publications Inc., 1955.
11. A. Gnedovets, A. Gusarov, and I. Smurov, "A model for nanoparticles synthesis by pulsed laser evaporation," *J. Phys. D: Appl. Phys.* **32**, pp. 2162–2168, 1999.
12. W. Vincenti and C. Kruger, *Introduction to Physical Gas Dynamics*, Krieger Publishing Company, 1965.
13. K. Suizu and K. Nagayama, "Cooling of pulsed laser-ablated plasma plume in an ambient gas and the onset condition of clustering in nanoparticle synthesis," *Applied Physics A* **69**, pp. S235–S238, 1999.
14. S. Botti, G. Cicognani, R. Coppola, A. Lapp, and M. Magnani, "Particle size and optical performances of photoluminescent laser synthesized si nanopowders," *Physica B* **276-278**, pp. 860–861, 2000.